Far-field seismogram perturbations induced by topographical heterogeneity

Stéphane Gaffet, B. Massinon

GEOPHYSICAL RESEARCH LETTERS, VOL. 24, NO. 24, PAGES 3313-3316, DECEMBER 15, 1997

Far-field seismogram perturbations induced by topographic heterogeneity

Stéphane Gaffet[1] and Bernard Massinon[2]

Abstract. The far-field contribution of the wavefield diffracted by topographical heterogeneities located in the vicinity of sources is analyzed in the case of nuclear explosions detonated inside the Taourirt Tan Afella massif, Algeria. The far-field scattered field is strongly shaped by the geometry of the topography and by the source location inside the mountain. Focusing and defocusing of the *pP* wave are shown. Back-scattering inside of the massif appears in the *coda* of the *pP* phase. For specific take-off angles, *ie* for given teleseismic distances, broadening of the *pS* diffracted field may appear. This broadening is explained by the simultaneous arrival of the *pS* and the *P* surface wave to *S* converted wave, with similar polarizations.

Introduction

The relation between crustal structures and far-field radiation is studied in the context of the Taourirt Tan Afella 1960s French nuclear test site on the Ahaggar plateau in Algeria. The location and topography of the granitic massif is depicted Fig. 1. The geological context has been described by Faure, small 1972, Boullier and Bertrand, small 1981, Duclaux and Michaud, small 1970, and Munier, small 1982. The present study analyses both radial and transverse displacement components emitted by the ground irregular topography in the source region with the aim of understanding waveform variations at different take-off angles for *Jade*, *Opale*, and *Rubis* nuclear tests (Table 1). Large amplitude variations occuring at local distances in relationship with the efficiency of Rayleigh wave generation by each side of the topographical heterogeneity was published in a previous paper (Gaffet *et al.*, small 1994). Our main objective here is to describe the topographic contribution of the far-field wavefield.

Study

Numerical simulations of synthetic seismograms are done using the discrete wavenumber - indirect boundary integral method (Gaffet and Bouchon, small 1989) for two topographic profiles along N0° and N100° azimuths. These 2D profiles cross the Tan Afella massif as depicted in Fig. 1. The closeness of the *Jade* and *Opale* explosions makes it possible to consider both sources as a single detonation point. In the aim of understanding the topography influence, we study the radial and transverse displacement fields diffracted by the surface ($\vec{u}_{diff}$). Thus, the 2D topographic *P-SV* seismograms displayed hereafter do not include the source free field ($\vec{u}_{free}$).

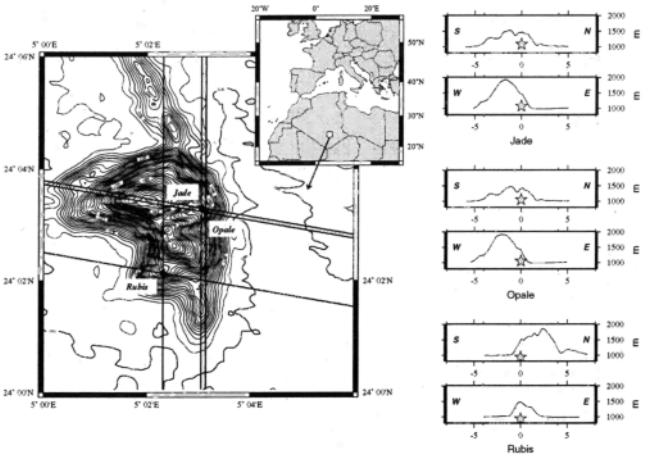

Figure 1. Geographic location of the 1960s French Nuclear Test site, location of the 3 explosions studied, and 2D topographical SN and WE profiles for *Jade*/*Opale* and *Rubis* explosions. The elevation and horizontal offset are given in meters and in kilometers respectively

$$\vec{u}_{total} = \vec{u}_{free} + \vec{u}_{diff} \quad (1)$$

The right side of Fig. 1 displays the 2D cross section configurations and the explosion locations used for the calculations. The *P* and *S* wave velocities are $\alpha = 5.3$ km/s and $\beta = \alpha/\sqrt{3}$ (Munier, small 1982). The maximum steepnesses of the topography are 29°, 32°, 35°, and 32° for *Jade* N0°, *Jade* N100°, *Rubis* N0°, and *Rubis* N100° respectively. The far-field influence analysis of source site effects deduced from numerical simulations performed with the reciprocity representation (Bouchon, small 1976, McLaughlin and Jih,

Table 1. Parameters of the studied explosions

Event	Date (UT time)	Lat N Lon E
Rubis USGS m_b=5.6	1963 10/20 13:00:00.011	24°2.130′ 5°2.317′
Opale	1964 02/14 11:00:00.347	24°3.218′ 5°3.143′
Jade	1965 05/30 11:00:00.037	24°3.300′ 5°3.052′

[1]UMR Géosciences Azur 6526 - 250, rue Albert Einstein - F-06560 Valbonne

[2]LDG - BP 12 - F-91680 Bruyères-le-Châtel

Paper number 97GL02977.
0094-8534/97/97GL-02977$05.00

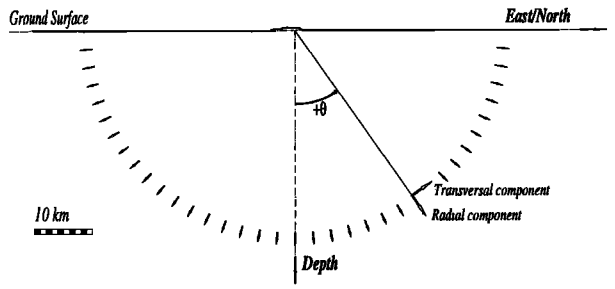

Figure 2. Geometry used for calculations. θ is the take-off angle positive toward the east and the north

small 1988, and Gaffet, small 1995), is not convenient to fully describe the contribution of the topographical heterogeneities to the far-wavefield because one calculation must be done for each take-off angle and for each component investigated.

Thus, instead of implementing such a huge computation approach, we here compute the radial and transverse seismograms at a radial distance of 35 km from the source area and for take-off angles ranging from 0° to 85° toward both sides of the topographical heterogeneity as displayed in Fig. 2. For each topographic cross-section the diffracted field is presented with a 5° take-off angle step for the two *Jade/Opale* and *Rubis* explosion configurations (Figs 3 and 4). This representation which does not include the t^* attenuation or the spalling effect is not, strickly speaking, the teleseismic field, but it appears to be a very useful way of understanding the origin of the different phases that may appear in the far-field wavefield.

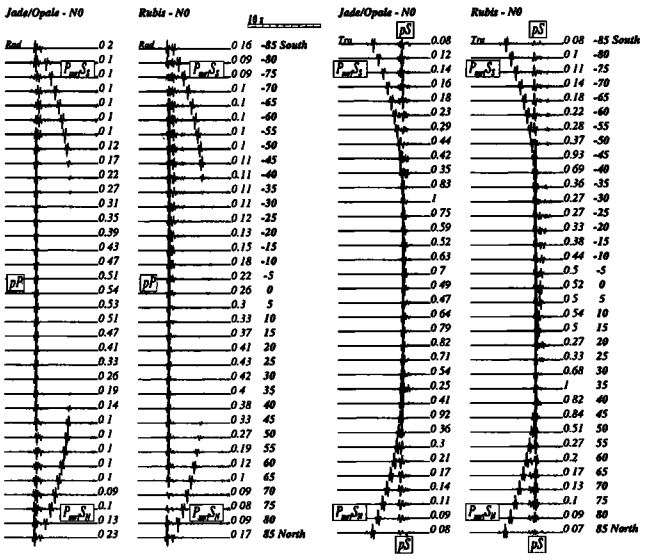

Figure 3. Radial and transverse field comparison for *Jade/Opale* and *Rubis* explosions at N0° cross-section. The seismograms are normalized for each component and their relative amplitude are written on the right side of each displacement stack. The take-off angle of the radial component is written in bold face characters from 0 (vertical incidence) to 85 (grazing incidence). The time duration is 13 seconds and the source time function is a Ricker pulse with a 3 Hz characteristic frequency

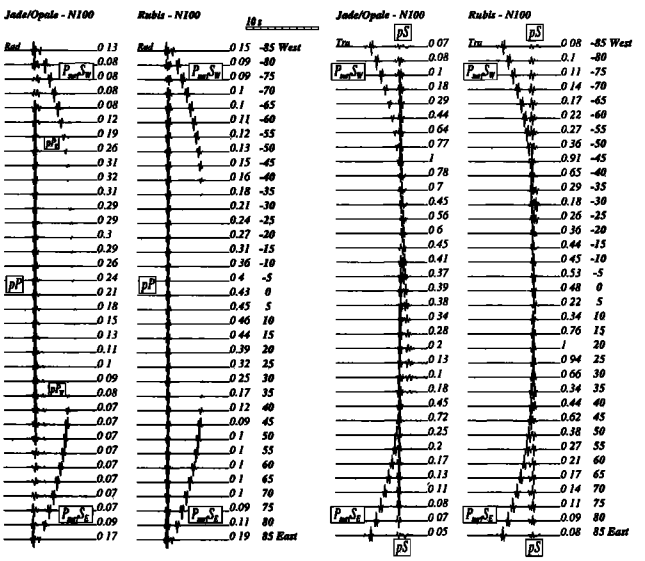

Figure 4. Same as Fig. 3 for the N100° cross-sections

N0° cross section

The seismograms displayed in Fig. 3 allow a comparison of the radial (2 left side columns) and transverse (2 right side columns) displacements for both the *Jade/Opale* and *Rubis* cases. The source P-wavelength is approximately one third the width of the mountain and twice its elevation.

For the *Jade/Opale* explosions, the southward amplitude diffracted in the 25° to 40° take-off range, is 25 to 35 % higher than the amplitude emitted symmetrically toward the north. This amplitude difference mainly applies to the pP wave which is then overestimated for the southern azimuths relative to the northern ones. This relative amplification may be explained by good geometrical reflexion conditions of the direct free field p up-going wave inside the northern flank of the mountain (Rocard, small 1964). In contrast, the northward radial diffracted field amplitude of the Rubis explosion, reaches up to 4 times the southward one over a broad range of take-off angles (*ie* between 5° to 55°).

The southern azimuthal amplitude attenuation is correlated to a lengthening of the pP wave shape compared to the northern one. Two non symmetrical branches (called $P_{surf}S_S$ and $P_{surf}S_N$) appear on the radial and on the transverse components for both explosions. These branches correspond to the P surface wave to S wave conversion (Lapwood, small 1949 and Bouchon, small 1978). The radial amplitude of these branches vanishes as the take-off angle decreases. They join the pS branch for take-off angles around 50°. The asymmetrical shapes of these branches are due to the asymmetrical propagation length of the P surface wave along the topography which results in different arrival times on opposite sides of the mountain.

The shape and amplitude variations of the diffracted transverse field are opposite for the *Jade/Opale* and *Rubis* experiments. This general behaviour is due to the opposite location of the explosion inside the mountain. Thus, take-off angles of 30° to 40° the southward transverse amplitude is 1.9 to 3.3 times the northward one for *Jade/Opale* while the

northward amplitude is 2.5 to 2.8 times the southward one for *Rubis*. The pS phase duration is longer and its content is enriched in higher frequencies for the southern azimuth compared to the northern one in the case of *Jade/Opale*. The opposite feature occurs for the *Rubis* explosion.

N100° cross section

The same type of calculations is presented in Fig. 4 for the N100° configuration. The characteristic source wavelength stays similar to the previous case for the *Jade/Opale* calculations. For the *Rubis* explosion, it is now about one half of the topographic width and 3 times its elevation.

The amplitude radiated for the *Jade/Opale* explosions is globally larger toward the west than toward the east for both the radial and transverse components. This behaviour is clearly related to a clear strong P reflexion of the free incident p wave field on the eastern flank of the Tan Afella massif. The relative amplification of the radial and transverse western seismograms reaches up to 4.5 times the amplitude of the eastern ones and concerns mainly the pP phase. In comparison to the N0° cross section, a larger number of branches appear for the *Jade/Opale* explosion on both the radial and transverse components. The *Rubis* field displays a simpler shape. The N0° previously observed branches are noted pP for the first arrivals and $P_{surf}S_W$ and $P_{surf}S_E$ for the later arrivals.

Two new phases are also generated and appear in the *coda* of the pP phase on the radial component: a clearly defined one noted pP_E and a subdued one noted pP_W for the *Jade/Opale* explosion. These $pP_{W,E}$ correspond to a double P reflexion of the incident free p wavefield inside the mountain. The low amplitude and the small time delay between the $pP_{W,E}$ and the pP phases are compatible with this hypothesis and correspond to the results deduced from local ground displacement simulations at the surface (Gaffet *et al.*, small 1994). For the *Jade/Opale* N100° explosion, a strong phase crosses the pS branch and can followed from the 10° westward azimuth to the 35° eastward azimuth. This branch extends the $P_{surf}S_W$ phase that can be seen on the radial component.

The simple field shape obtained for *Rubis* may be related to the smaller size of the massif compared to the *Jade/Opale* configuration. Nevertheless some discrepancies are found between the shape of the pP field diffracted from *Jade/Opale* and from *Rubis* for ranges of take-off angles from W70° to W75° and from E55° to E70°. For these take-off angles, the pP phase induced by the *Jade/Opale* explosion has a lower amplitude and a lower characteristic frequency than the pP phase generated by *Rubis*.

Phase polarization and characterization

Fig. 5 displays the polarization diagram for the studied configurations. This presentation allows a clear understanding of the origin of the $P_{surf}S$ wave type. For all explosions, cross-sections, and take-off angles for which it appears, the $P_{surf}S$ phase shows a constant polarization angle for western and eastern take-off angles ranging from 50° to 85°. The

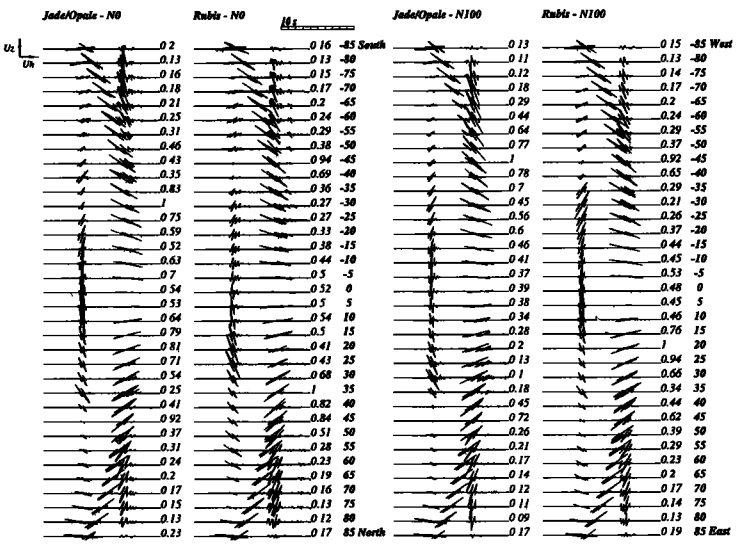

Figure 5. Polarization diagram corresponding to a time domain extension of the particle motion for *Jade/Opale* and *Rubis* explosion and for the N0° and N100° cross-sections. The relative amplitudes of the displacement modulus are written to the right side of each column

sine of this angle is equal to the wave velocity ratio β / α of the propagation model. Thus, this angle confirms that the origin of the corresponding phase is a P surface wave to S conversion as previously assumed. The polarization diagram also shows that this phase vanishes with near-vertical take-off angles. This is well illustrated for the western azimuth of the *Jade/Opale* N100° column (Fig. 5).

A defocusing area appears for the *Jade/Opale* N0° configuration between 35° and 40° and mainly concerns the pS phase. In comparison to the eastern azimuths, both the P and S diffracted fields are enhanced in the western azimuth for the *Jade/Opale* N100° cross-section. A focusing of the pS wave appears eastward for a 45° take-off angle.

The global relative amplification of the northward diffracted pP phase and the global increase in time duration of the southward diffracted pP phase for the *Rubis* N0° cross-section is not related to any special feature of the pS wave. On one hand, no special behaviour can be observed concerning the pP phase for the *Rubis* N100° configuration. On the other hand, an amplification of the pS wave appears for a 45° westward take-off angle. This may be related to the combination of the $P_{surf}S_S$ and pS phases. This phase combination enhancement appears to be the main mechanism to explain the amplification of the S field for all configurations at take-off angles around 45°. Finally we may note that the surface Rayleigh wave appears behind the pS phase at grazing take-off angles (close to 90°).

Fig. 6 summarizes the amplification or deamplification behaviours described previously and compares the maximum amplitude of the radial and transverse components (left and right sides respectively) for the *Jade/Opale* and *Rubis* explosions at N0° and N100° cross-sections as a function of the take-off angle. The length of each ray is related to the maximum amplitude determined from the radial

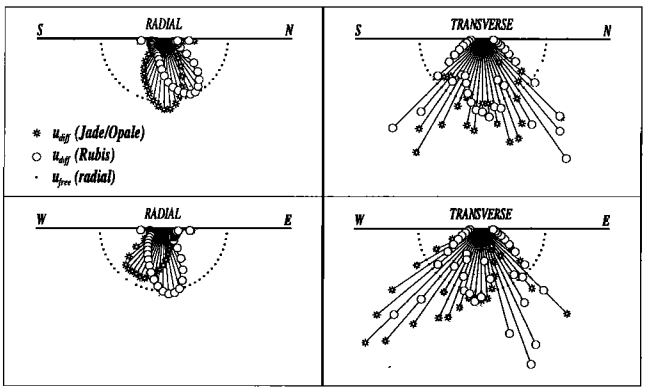

Figure 6. Maximum amplitude for the radial and transverse components for *Jade/Opale* and *Rubis* explosions at N0° and N100° cross-sections as a function of the take-off angle. Black dots correspond to the radial displacement of the source in a infinite homogeneous space ($\vec{u}_{free}$, eq. 1). White stars and circles correspond to the field diffracted by the topography for *Jade/Opale* and *Rubis* explosions respectively ($\vec{u}_{diff}$, eq. 1)

and transverse seismograms. The main observation concerns the regular variation of the maximum amplitude of the radial component in comparison to the great variability of the transverse maximum amplitudes with take-off angle. The regularity of the former is directly related to the pP phase that mainly shapes the radial seismograms without interferences with the $P_{surf}S$ phases, while strong interferences occurs between $P_{surf}S$ and pS branches for the transversal component at specific take-off angles that depend on the explosion configurations.

Conclusion

Using numerical discrete wavenumber - indirect boundary integral simulations, we describe the elastic field diffracted by a mountain heterogeneity towards far-field distances. The influence of the heterogeneous topography on the classical pP and pS wave shapes may be summarized as defocusing and amplification effects. These effects are clearly related to the reflection coefficient of the incident free p wavefield on the massif surface. Specific phases that correspond to P surface wave to S conversion are shown. The corresponding branches vanish for near-vertical incidences. Backscattering inside the mountain may generate secondary pP branches that enhance the *coda* of the main pP wave. A specific amplification process is shown which results from the combination of the P surface to S wave conversion and of the pS waves. The related amplification occurs when simultanecusly the $P_{surf}S$ and pS polarizations become similar and when the corresponding $P_{surf}S$ and pS branches intersect. Finally, the teleseismic pP-waves with take-off angles of less than 20° show amplitude variability of about a factor of 2 due to different locations within the mountain and take-off angles. Likewise, the variations in pS are about a factor of 2 to 3. The predicted teleseismic pP variations are thus consistent with those predicted by McLaughlin and Jih, small 1988 using another numerical simulation method.

Acknowledgments. This work was supported by the Laboratoire de Détection et de Géophysique of the French Commissariat à l'Énergie Atomique. Numerical calculation were performed with the CRAY computers of the French Institut du Développement et des Ressources en Informatique Scientifiques (IDRIS/ CNRS). We are grateful to the reviewers for their fruitful comments on the manuscript. Publication of the *UMR CNRS 6526 - Géosciences Azur* n° 145.

References

Bouchon, M., teleseismic body wave radiation from a seismic source in a layered medium, *Geophys. J. R. astr.*, 47, 515–530, 1976.

Bouchon, M., the importance of the surface or interface p wave in near-earthquake studies, *Bull. Seism. Soc. Am.*, 68, 1293–1311, 1978.

Boullier, A.-M., and Bertrand, J.-M., tectonique tangentielle profonde et couloirs mylonitiques dans le hoggar central polycyclique (algérie), *Bull. Soc. géol. France*, 33, 17–22, 1981.

Duclaux, F., and Michaud, L., conditions expérimentales des tirs nucléaires souterrains français, 1961-1966, *C. R. Acad. Sc. Paris*, 270, 189–192, 1970.

Faure, J., recherche sur les effets géologiques d'explosions nucléaires souteraines dans un massif de granite saharien, *CEA Report*, CEA-R-4257, 1–273, 1972.

Gaffet, S., and Bouchon, M., effects of two-dimensional topographies using the discrete wavenumber - boundary integral equation method in p-sv cases, *J. Acoust. Soc. Am.*, 85, 2277–2283, 1989.

Gaffet, S., Massinon, B., Plantet, J.-L., and Cansi, Y., modelling local seismograms of french nuclear tests in taourirt tan afella massif, hoggar, algeria, *Geophys. J. Int.*, 119, 964–974, 1994.

Gaffet, S., teleseismic waveform modeling including geometrical effects of superficial geological structures near to seismic sources, *Bull. Seism. Soc. Am.*, 85, 1068–1079, 1995.

Lapwood, E., the disturbance due to a line source in a semi-infinite elastic medium, *Phil. Trans. Roy. Soc. London Ser.*, A242, 63–100, 1949.

McLaughlin, K., and Jih, R.-S., scaterring from near-source topography: teleseismic observations and numerical simulations, *Bull Seism. Soc. Am.*, 78, 1399–1414, 1988.

Munier, G., construction d'un modèle de croûte sous le hoggar central, *CEA Report*, CEA/LDG 53-82, 1–125, 1982.

Rocard, Y., formation du signal séismique lors d'une explosion souterraine, *C. R. Acad. Sc. Paris*, 258, 2373–2375, 1964.

S. Gaffet, UMR Géosciences Azur 6526, 250 rue Albert Einstein, F-06560 Valbonne (e-mail:gaffet@faille.unice.fr)

B. Massinon, CEA/LDG, BP 12, F-91680 Bruyères-le-Châtel

(Received January 6, 1997; revised September 18, 1997; accepted October 3, 1997.)